

Counting individual galaxies from deep 24 μm Spitzer surveys: beyond the confusion limit

G. Rodighiero¹, C. Lari², F. Pozzi^{3,4}, C. Gruppioni⁴, D. Fadda⁵, A. Franceschini¹, C. Lonsdale⁶, J. Surace⁶, D. Shupe⁶ and F. Fang⁶

¹*Dipartimento di Astronomia, Università di Padova, Vicolo dell'Osservatorio 5, 351 22 Padova, Italy*

²*Istituto di Radioastronomia del CNR, via Gobetti 101, I-40129 Bologna, Italy*

³*Dipartimento di Astronomia, Università di Bologna, via Ranzani 1, I-40127 Bologna, Italy*

⁴*Istituto nazionale di Astrofisica, Osservatorio Astronomico di Bologna, via Ranzani, I-40127 Bologna, Italy*

⁵*Spitzer Science Center, California Institute of Technology, MC 220-6, Pasadena, CA 91125*

⁶*Infrared Processing and Analysis Center, California Institute of Technology, MC 100-22, Pasadena, CA 91125*

14 December 2018

ABSTRACT

We address the question of how to deal with confusion limited surveys in the mid-infrared domain by using informations from higher frequency observations over the same sky regions. Such informations, once applied to apparently extended mid-infrared sources, which are indeed “blends” of two or more different sources, allow us to disentangle the single counterparts and to split the measured flux density into different components. We present the application of this method to the 24 μm *Spitzer* archival data in the GOODS-EN1 test field, where apparently extended, “blended” sources constitute about 20% of a reliable sample of 983 sources detected above the 5σ threshold down to 23 μJy . As higher frequency data-set we have considered the public IRAC images and catalogues on the same field. We show that the 24 μm sample is almost unbiased down to ~ 40 μJy and the careful application of the deblending procedure does not require any statistical completeness correction (at least at the flux level considered). This is probed by direct comparison of our results with those of Chary et al. (2004), who analysed the same data-set through extensive Monte Carlo simulations. The deblending procedure reduces of about 30% the confusion limit of the MIPS 24 μm survey, allowing one to obtain reliable source counts down to ~ 40 μJy . The extrapolation of the source counts down to fainter fluxes suggests that our 24 μm sample is able to resolve $\sim 62\%$ of the cosmic background down to a flux level of 38 μJy .

Key words:

infrared: general – infrared: galaxies – galaxies: photometry – method: data analysis – catalogues

1 INTRODUCTION

Cosmological surveys in the Mid-Infrared (MIR) / Far-Infrared (FIR) spectral range reveal a substantial population of strongly evolving dust-enshrouded galaxies at intermediate redshifts (e.g. Elbaz et al. 1999; Franceschini et al. 2003). These galaxies are responsible for most of the cosmic infrared background detected at these wavelengths (CIRB, Hauser & Dwek 2001). Although a significant fraction of the CIRB is already resolved into discrete sources by deep infrared surveys (i.e. ISOCAM have resolved about 60-70% of the CIRB at 15 μm), to resolve the whole observed background light we should reach fainter flux limits.

However, the main limitation of deep surveys performed in the MIR/FIR domain is confusion due to extragalactic

sources. In fact, the large number of distant galaxies in deep extragalactic surveys produces a high density of sources with respect to the instrument beam size. This makes more than one source responsible for the measured flux density at the fainter limits, therefore producing wrong source counts (i.e. higher than real at intermediate flux densities due to source “blending”) and limiting the effective survey sensitivity.

As recently suggested by Dole et al. (2005), we will show that it is possible to deal with this problem, significantly lowering the confusion limit in deep extragalactic surveys by making use of higher frequency observations on the same region of the sky. In particular, data obtained with the Infrared Array Camera (IRAC; Fazio et al. 2004) on board of *Spitzer* in the 3.6 to 8.0 μm wave-bands are extremely helpful for measuring fluxes of faint sources and reducing

the confusion noise in surveys performed with the *Spitzer* Multiband Imaging Photometer (MIPS; Rieke et al. 2004) at 24, 70 or 160 μm . Through IRAC data, we have developed an efficient “deblending” technique that allows us to accurately measure the flux density of sources detected by MIPS below the nominal confusion limit and therefore to significantly lower this limit (of about 30–50%). The application of this technique to the GOODS ELAIS-N1 (EN1) test field is presented in this paper.

The paper is structured as follows: in section 2 we present the observations in the GOODS-EN1 field; in section 3 we describe the 24 μm data processing and we present the 24 μm catalogue, while in section 4 we discuss the “deblending” technique; in section 5 we show the number counts; in section 6 we present our conclusions.

Throughout this paper we will assume $H_0 = 75 \text{ km s}^{-1} \text{ Mpc}^{-1}$, $\Omega_m = 0.3$ and $\Omega_\Lambda = 0.7$.

2 OBSERVATIONS

The EN1 field is one of the best areas, among the currently available ones, for investigating the effects of source confusion in MIR surveys. Deep MIPS 24- μm observations in this field cover an area of $\sim 185 \text{ arcmin}^2$ (centred at 16:09:20 +54:57:00) as part of the Great Observatories Origins Deep Survey (GOODS) Science Verification program of *Spitzer*. The field was observed in photometry mode. Two different AORs were executed in cluster mode using the offset position in order to symmetrically observe one side of the field. The integration time per detector pixel varies from $\sim 2000 \text{ s}$, in the lowest signal to noise area, up to $\sim 4600 \text{ s}$ in the deepest regions. Details on the MIPS 24- μm data processing, source extraction and photometry will be given in the next section.

Although during the same verification observing campaign complementary deep NIR observations of EN1 have been obtained with IRAC with the 3.6, 4.5, 5.8 and 8.0 μm channels, the combined IRAC GOODS maps do not perfectly overlap the whole MIPS GOODS image, thus leaving a fraction of the MIR map uncovered by NIR data. However, a shallower and more extended observation of EN1 with the four IRAC channels has been performed as part of the SWIRE Legacy programme (Lonsdale et al. 2003), covering a much wider area ($4 \times 4 \text{ deg}^2$), and thus homogeneously overlapping the deeper GOODS verification MIPS data. We therefore used the SWIRE map at 3.6 μm to have a complete NIR coverage of our MIPS image.

Optical imaging of the GOODS EN1 field is provided by the First Look Survey (FLS) observations (Fadda et al., 2004). The R-band images were obtained using the Mosaic-1 camera on the 4 m Mayall Telescope of the Kitt Peak National Observatory. The images reach a median 5σ depth limiting magnitude of $R = 25.5$ (Vega) as measured within a 1.35 FWHM aperture, for which the signal-to-noise ratio is maximal.

2.1 IRAC data processing

The reduction of GOODS data in the IRAC bands has been performed by starting from the basic calibrated data (BCD)

obtained from the *Spitzer* archive. We have applied an additive correction factor to each BCD frame in order to remove the median background. We have then processed and mosaiced together all the corrected BCDs with the *Spitzer* Mopex package¹ version distributed on June 2004 by the Spitzer Science Center (SSC). We refer to Lonsdale et al. (2004) for a complete description of the observation strategy and data analysis of SWIRE.

The IRAC source extraction has been performed with SExtractor (Bertin & Arnouts, 1996), both on SWIRE and GOODS maps. For point-like sources, we computed the fluxes within a 6 arcsec diameter aperture. We have then applied a correction factor derived from the stars in the images to obtain the total fluxes (1.14). In the case of extended sources, we used Kron like magnitudes (AUTO_MAG output parameter in SExtractor). The IRAC photometry has been basically used to remove stars in the 24 μm catalogue.

3 MIPS 24 μm DATA PROCESSING

3.1 Mosaic generation and manipulation

We started the data analysis of the 24 μm data in the GOODS EN1 field from the archival BCD products. These have been pre-processed using version S10.0.3 of the SSC pipeline (see *Spitzer* Observer Manual). Firstly, we have corrected each single BCD frame by computing a residual median flat-field which depends on the scan mirror position. Such flat-field has been built from the data.

By checking the temporal histories of each pixel we observed a non-linear response of the detector, that does not instantly reach the stabilization level. This produces a transient on the observed time sequence of MIPS pixels. We corrected this effect by applying a linear fit to the temporal sequence of each pixel. As stabilization level we choose the value of the final exposure frame. With this procedure we produced background subtracted and flat-fielded frames that were co-added using the SSC software Mopex to obtain a mosaic with half the original pixel scale (1.2 arcsec).

The projection algorithm applies a linear interpolation that accounts for the distortion corrections. Bad pixels are masked within the pipeline and cosmic rays are flagged using a multiframe temporal outlier detection. The signal-to-noise map of the EN1 GOODS field observed by MIPS is shown in Figure 1.

In order to remove the Airy rings around sources we have deconvolved the 24 μm image using the CLEAN task (typically used for analysing radio data), which is part of the NRAO AIPS reduction package. The CLEAN algorithm iteratively finds and subtracts positive features on the original map until the standard deviation of the residual image is lower than the noise level. The CLEAN map is then constructed by adding to the residual image the CLEAN components found, convolved with a Gaussian of FWHM that is equal to that of the MIPS 24 μm PSF (we computed a value of 5.5 arcsec by fitting the PSF provided with the used version of Mopex). This gaussian beam is normalized to one in the peak, and the ratio between its total flux and that of

¹ See <http://ssc.spitzer.caltech.edu/postbcd>.

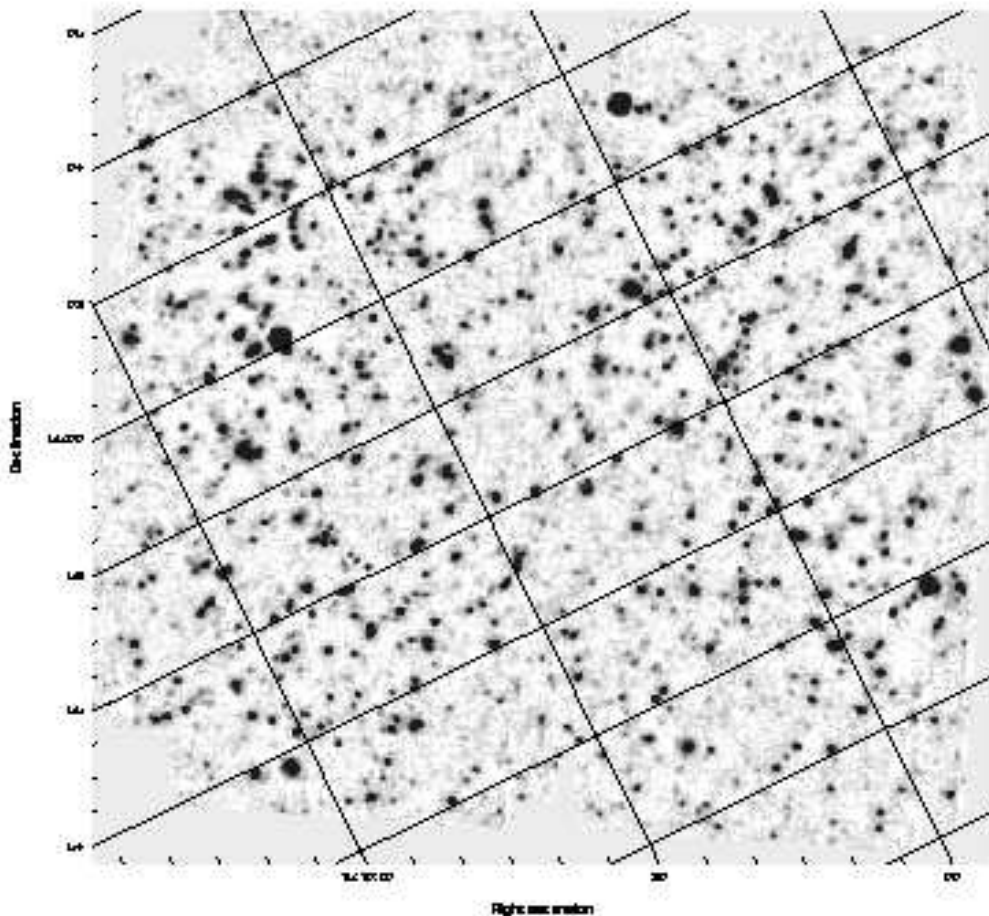


Figure 1. Signal to noise map of the deep EN1 field observed by MIPS.

the original MIPS PSF is 1.369. For construction, this factor represents also the ratio between the equivalent areas of the original PSF and the restored gaussian beam, in spite of having the same FWHM. In other words, the Spitzer PSF affects a larger area of the sky and suffers of a greater confusion. The mentioned procedure allows us to obtain a map (the CLEAN map) where the Airy rings are removed.

An example of the effects of applying the CLEAN procedure is illustrated in Figure 2, where we report a zoom of 2.2×1.4 square arcminutes into the map presented in Figure 1. The upper panel shows the original flux map, in the lower panel the corresponding cleaned map shows that the adopted approach is efficient in deconvolving many close sources, providing a reconstructed map where the confusion due to first Airy ring is reduced. We will show that this procedure is not sufficient to solve most of the confusion, and that a more accurate approach to deal with these cases is needed.

3.2 Source Extraction

Before performing source extraction, we have applied a recursive median filtering to the final mosaic map. The size of the box used to compute the median is 64×64 pixels of

1.2 arcsec. This procedure is used in order to smooth residual spurious background fluctuations. Source detection is then performed on the signal-to-noise map by selecting all pixels above a low flux threshold ($0.5\ \mu\text{Jy pixel}^{-1}$) using the IDL Astronomy Users Library routine called *find* (based on DAOPHOT's equivalent algorithm). We then extract from the detection list only the objects with signal-to-noise ratio greater than 5. The preliminary list includes 953 sources. The combination of long exposure times and high repetition factor of this Spitzer survey provides a very deep infrared observation of the sky, that is basically confusion limited. For this reason we checked each detected source by visual inspection. We exploited the availability of higher frequency observations from IRAC (see section 2) to look for the counterparts of eventual blended MIPS sources. Indeed, the better resolution of the Spitzer near-IR data allows one to disentangle the multiple components of the mid-IR sources. We found that 21% of 953 sources are “blended”. These objects have generally pairs or small groups as NIR/optical counterparts. A representative sample of this class is shown in Figure 3, where for each blend case we report both NIR (IRAC 3.6, left panel) and optical (R band, right panel) images overlaid with the MIPS $24\ \mu\text{m}$ contours ($> 3 - \sigma$).

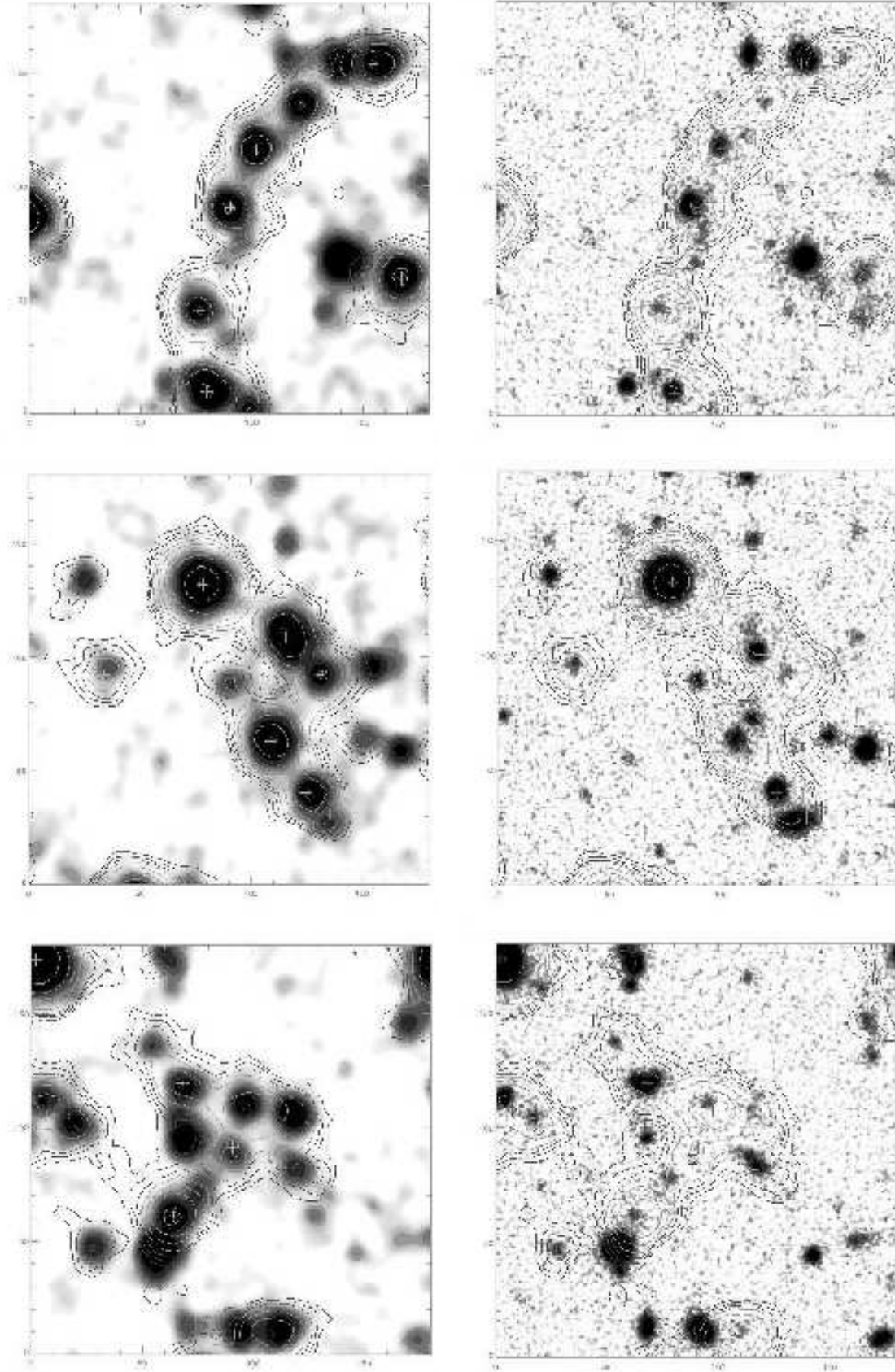


Figure 3. Example of three blend $24\ \mu\text{m}$ sources. For each case we report both the near-IR (IRAC $3.6\ \mu\text{m}$, left panel) and the optical (R band, right panel) images overlaid with the MIPS $24\ \mu\text{m}$ contours, starting from the 2-sigma level at increasing values. North is up, East at left. Each image is 50×50 arcsec. The crosses mark the positions of the $24\ \mu\text{m}$ sources in the catalogue with signal-to-noise ratio

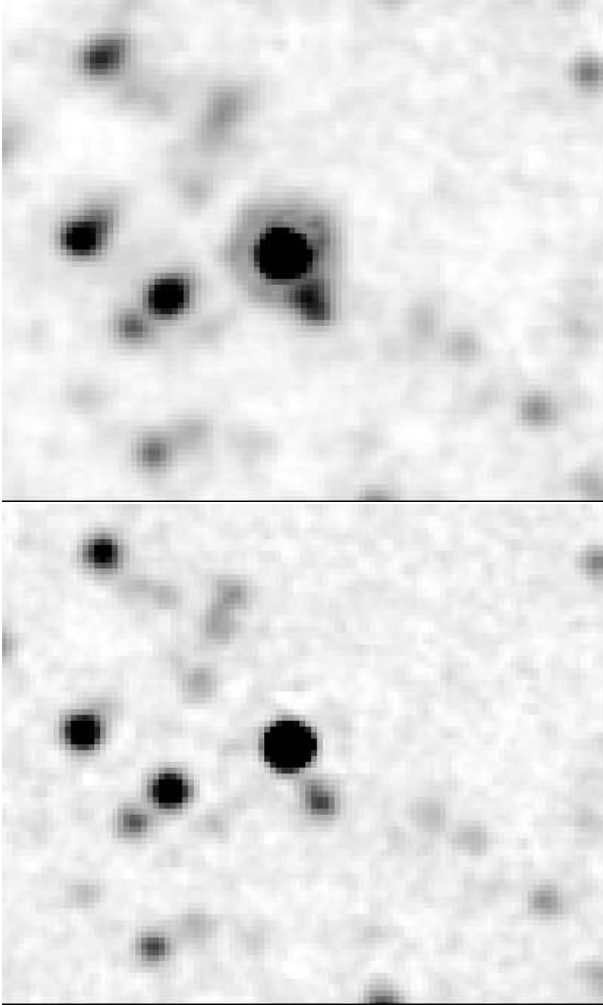


Figure 2. Example of the effects of applying the CLEAN task to the flux map. We report a zoom of 2.2×1.4 square arcminutes into the map presented in Figure 1. The upper panel shows the original flux map, in the lower panel the corresponding cleaned map shows that the adopted approach is efficient in deconvolving many close sources, providing a reconstructed map where the confusion due to first Airy ring.

3.3 Photometry

Since most of the objects in our catalogue are faint point-like sources, their $24\ \mu\text{m}$ flux density is computed by applying a correction factor to the measured peak flux, in order to convert the peak flux into a total flux density. The correction factor is basically computed from the *Spitzer* MIPS PSF, provided within the Mopex package (as of June 2004), and is found to have a value of 32.5. However, other authors report slightly different aperture corrections, which are taken into account when comparing the source counts (see Section 5). In this work the standard calibration from the SSC is applied. Future detailed measures of stellar fluxes, to be compared with atmosphere model predictions, will provide a more robust absolute calibration for Spitzer photometry. The MIPS $24\ \mu\text{m}$ absolute flux calibration is correct within few percent.

The measure of the total flux from its peak value has been applied to every isolated source. For the few extended

sources (three) aperture photometry was computed. A different approach is required in the case of confused and blended sources. We have examined each single MIPS blend source and determined the multi-counterparts looking at the IRAC image. When the associations are not clear, we refer to the optical R band frames that allow us to visually check and solve most of the ambiguous cases. Once the number and the positions of the counterparts of a mid-IR blend source are fixed, a PSF fitting algorithm (IMFIT, within the AIPS environment) was applied to compute an accurate photometric deblending on the CLEAN map. Blended sources are assumed to be point like sources. This provides a measure of the $24\ \mu\text{m}$ flux of each confused component. At the end of this analysis the final MIPS sample in the GOODS EN1 field includes 983 sources detected above the 5σ threshold.

3.4 The $24\ \mu\text{m}$ GOODS EN1 catalogue

The adopted deblending procedure turns out to be an efficient tool to break through the confusion limit of the deep MIPS $24\ \mu\text{m}$ surveys, such as GOODS. The use of combined higher frequency maps (near-IR and optical in our case) has allowed us to build an unbiased sample of faint IR sources. This will be discussed in more detail in Section 4.

As an illustration, in Table 1 we report a tabulation of the first 10 rows of the final catalogue of $24\ \mu\text{m}$ detections in the GOODS EN1 validation field. The complete catalogue² contains 983 sources detected above 5σ and down to a minimum flux level of $23\ \mu\text{Jy}$. The five entries in the Table are: IAU source designation, right ascension and declination (J2000), signal-to-noise ratio, total $24\ \mu\text{m}$ flux density (in μJy). Fluxes marked on the right side with an asterisk indicate the 11 sources classified as stars. Figure 4 shows the distribution of the $S(24\mu\text{m})/S(3.6\mu\text{m})$ flux ratio as a function of the $24\ \mu\text{m}$ flux for the sources in the final catalogue. This near-to-mid IR colour is an efficient star/galaxy separator (a similar technique was already used by us for 15 μm ISOCAM sources, Rodighiero et al. 2004). The dashed horizontal line marks the Rayleigh-Jeans ratio. We classified as stars all sources with $S(24\mu\text{m})/S(3.6\mu\text{m}) < 0.1$. The few points above the dashed line correspond to elliptical galaxies.

The flux uncertainties are basically given by the signal-to-noise ratio.

4 EFFECTS OF CONFUSION

To quantitatively estimate the global effect of confusion in the EN1 GOODS $24\ \mu\text{m}$ map, we have measured the density of galaxy pairs at increasing distance scale. The result is shown in Figure 5.

For each single source we have counted the number of detections falling within a circle of radius r centered on the source position. This is recursively done for different increasing values of r , and for all the sources in the catalogue.

² The complete catalogue in ASCII format is made publicly available through the world-wide-web: <http://dipastro.pd.astro.it/giulia/EN1/ver> or directly on request the authors.

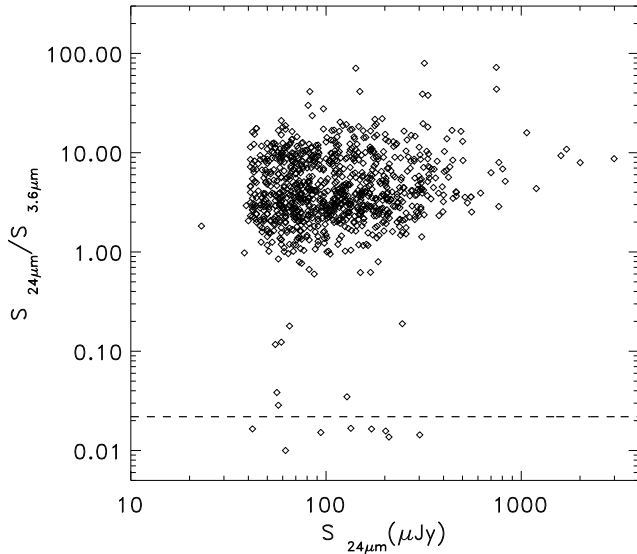


Figure 4. $S(24\mu\text{m})/S(3.6\mu\text{m})$ flux ratio as a function of the $24\mu\text{m}$ flux for the sources in the final catalogue. The dashed horizontal line marks the Rayleigh-Jeans ratio. We classified as stars all sources with $S(24\mu\text{m})/S(3.6\mu\text{m}) < 0.1$.

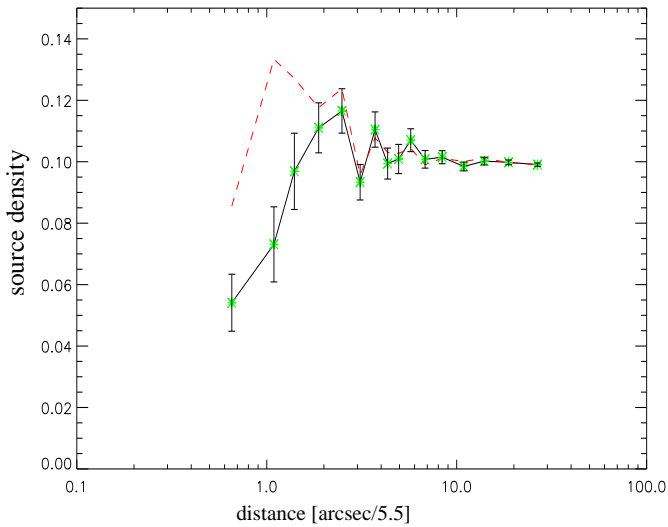


Figure 5. Number of detections falling within a circle of radius r (centered on the source position) normalized to a circular area with radius of $5.5''$, as a function of distance r for all the sources in the catalogue. The solid line represents the preliminar $5\text{-}\sigma$ catalogue before deblending the confused sources (it includes 953 sources), while the dashed line has been built from the final deblended catalogue (983 sources). No corrections were applied for the variable noise, but only for the geometry as the larger circles are limited by

The median value of the source density at each distance r is normalized to a circular area with radius of $5.5''$, and plotted against r . The solid line in the figure is computed using the preliminar $5\text{-}\sigma$ catalogue before deblending the confused sources (it includes 953 sources), while the dashed line has been built from the final deblended catalogue (983 sources). No corrections were applied for the variable noise, but only for the geometry as the larger circles are limited by

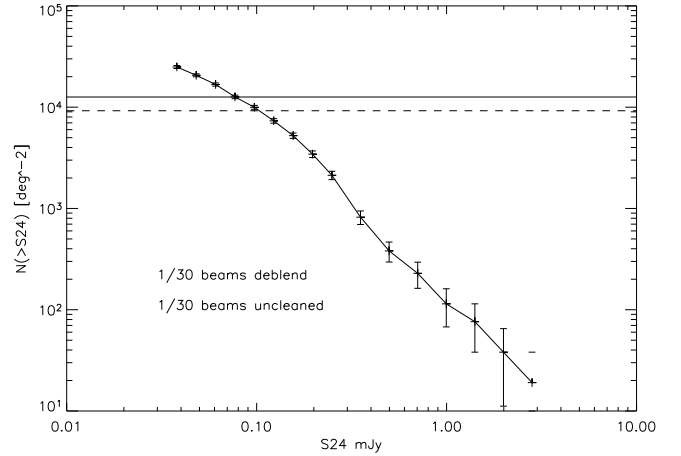


Figure 6. Final integral source counts (computed as described in Section 5 from the deblended catalogue). The horizontal lines mark the level at which the classical confusion noise is reached (30 beams per source, Condon et al. 1974). The solid line is computed by using the CLEAN gaussian beam, while the dashed line is derived from the standard PSF beam.

the boundary of the map. This analysis indicates the completeness of our method: the only sources that we are not able to deblend only those too close to each other (angular separation lower than $\sim 6''$). Obviously, identifications from higher resolution instruments may help, but if the separation is too small, even IRAC observations might suffer of confusion problems. A Montecarlo simulation test can recover these small deficits when dealing with source counts, however we have been very conservative when computing the source counts, cutting at a flux level which is not affected by the mentioned problem.

We have directly measured the confusion level of the $24\mu\text{m}$ observations from the observed cumulative source counts. This is presented in Figure 6 where we show our final integral source counts (computed as described in Section 5 from the deblended catalogue). The horizontal lines mark the level at which the classical confusion noise is reached (30 beams per source, Condon et al. 1974). The solid line is computed by using the CLEAN gaussian beam, while the dashed line is derived from the standard PSF beam (the latter being a factor of 1.369 greater than the former, see Section 3.2). This result confirms that the approach of using higher frequency to constrain the multi-counterparts of the blend/confused mid-IR sources is successful in reducing the intrinsic confusion limit of deep mid-IR maps. In particular, we have obtained $24\mu\text{m}$ confusion limits of $77\mu\text{Jy}$ and $103\mu\text{Jy}$ from the final and the pre-cleaned samples respectively. The confusion limit is then decreased of about 30%. These values are consistent with those extrapolated from model predictions by Dole et al. (2004). They report three different estimates based on different methods: $56\mu\text{Jy}$ (from the source density criterion, Dole et al. 2003), 71 and $141\mu\text{Jy}$ (levels deduced from the source density of one source per 20 and 40 independent beams).

5 EXTRAGALACTIC NUMBER COUNTS

To study the statistical properties of our sample, and to alternatively check the effects of confusion on our results, we have computed the extragalactic source number counts. Stars were removed from this compilation. We have computed the 24 μm source counts down to a flux level of $\sim 30 \mu\text{Jy}$. The counts have been obtained by weighting each single source for the effective area corresponding to its flux density.

In Figure 7 we report the differential 24 μm counts normalized to the Euclidean law ($dN/dS \propto S^{-2.5}$). We compare the distribution obtained by using our final deblended catalogue (filled circles, 983 sources) and the preliminary 5- σ catalogue obtained before deblending (open circles, 953 sources). The errors associated to the counts have been computed as $\sqrt{\sum_i 1/A_{eff}^2(S_i)}$, where the sum is for all the sources with flux density S_i and $A_{eff}(S_i)$ is the effective area corresponding to that flux. The quoted errors have to be considered as lower limits of the total errors.

The two distributions reported in Figure 7 clearly show that, when accounting for confusion, the density of faint sources is generally increased, and the source counts slope is less steep (by a factor of ~ 2) below the peak observed at $\sim 0.2 \text{ mJy}$.

In section 4 we argued that an accurate deblending analysis might provide un-biased complete samples. This is quantitatively confirmed if we compare our results with those derived by Chary et al. (2004), starting from the same data-set in the EN1 GOODS 24 μm field, while they have not treated each single source by looking at the counterparts in the IRAC map. They have followed a statistical approach to study the properties of the 24 μm population. Their completeness corrections were measured using a Monte Carlo approach: by adding artificial sources on the original mosaic, they were able to recover the fraction of undetected/lost sources as a function of the flux level combined with their extraction procedure. In Figure 7 we report also the source counts by Chary et al. (2004) for comparison with our estimate. The filled triangles refer to their uncorrected counts, while the open ones correspond to their final completeness corrected data.

We have mentioned (Section 3.3) that to compare our data with those from other authors we need to apply a correction factor to report the different results to the same flux scale. For consistency, we have firstly scaled upward by a factor of 1.057 the fluxes of our sources. This factor is needed to recover the light lost in the outer PSF lobes, and it has been computed as the ratio between the integral of the PSF and the flux of the same PSF measured within an aperture of $37.4''$. We have not applied this correction to the fluxes presented in the final catalog, as it has been derived from a theoretical PSF and should instead be better constrained from an absolute calibration based on atmospheric stellar emission models compared to the observations. Chary et al. (2004) have computed the flux of a source in a circular aperture of radius $6''$ and corrected upward by a factor of 1.8 to account for the wings of the PSF. Using the PSF derived in this paper (see Section 3.3) we found that the factor to convert $6''$ aperture fluxes to total fluxes is about 1.45. This implies that we need to correct the fluxes in the source counts reported by Chary et al. (2004) downwards by a factor $1.8/1.45=1.24$ to compare them with our estimates

on the same scale. A reason for this discrepancy may rely on the PSF provided by Mopex (at least for the version of June 2004 used in this work), which is not extended enough to recover the total flux lost in its wide wings. This is confirmed by testing the correction factor at the same aperture considered by Chary et al., $6''$, using a different PSF, computed with Spitzer/TINYTIM by Fadda et al (2005, in prep.) and that is quite similar to that measured from a real star in the First Look Survey (D. Fadda 2005, private communication). The aperture correction in this case is 1.76, very close to the 1.8 factor reported by Chary et al. (2004).

Once the flux scale correction is applied, the comparison between Chary et al. counts and ours shows a remarkable consistency (see Figure 7). This result is a direct demonstration that we do not need to apply any statistical correction to our sample, which turns out to be almost un-biased down to relatively faint fluxes ($40 \mu\text{Jy}$).

A major advantage of having carefully accounted for the contribution of confused sources, is that we have produced a catalogue which is not only suited for statistical purposes, but also to study the spectro-photometric properties of the single faint mid-IR sources.

In Figure 8 in addition to comparing our source counts (filled circles) to those of Chary et al. (2004, open triangles), we show also those from Papovich et al. (2004, filled triangles). As for the case of Chary et al. counts, we have applied a correction factor to the data of Papovich et al. (2004). Their source photometry corresponds to the flux of a PSF (derived from the bright stars in the field) within an aperture diameter of $37''.4$, then they apply a multiplicative correction of 1.14 to account for light lost outside this aperture. From our “edge cut” PSF we find that a $37''.4$ aperture flux is a good measure of the total flux. This implies that we need to correct downward by a factor $1.14/1.0=1.14$ the fluxes in the source counts of Papovich et al. (2004) to bring them on the same scale as ours.

We also report the 24 μm counts published by Marleau et al. (2004, open circles). They use a correction of 1.1 (D. Fadda, priv. comm.) to compute the total flux from an aperture photometry of radius $15.24''$. At the same aperture we compute a correction factor of 1.09. The scaling factor to be applied to Marleau et al. counts, in order to have them referred to our flux scale, is then very small, $1.1/1.09=1.01$.

Although Figure 8 shows a general agreement between the four independent 24 μm counts analysis over about a decade in flux (at low fluxes: $0.03 \text{ mJy} - 0.3 \text{ mJy}$), at fluxes brighter than 0.3 mJy the GOODS N1 statistics is quite poor as the field was explicitly chosen to avoid bright mid-IR sources (based on the positions of ISOCAM sources). The study of Papovich et al. (2004) is based on a much wider area ($\sim 10 \text{ deg}^2$), splitted in different sky regions. Poor statistics and cosmic variance on small scales (as the size of the EN1 field) can be the reason for the counts discrepancy observed above 0.3 mJy .

By integrating our source counts down to $S(24 \mu\text{m})=38 \mu\text{Jy}$ we have obtained an estimate of the 24 μm cosmic background intensity down to that flux level: $1.25 \text{ nWm}^{-2}\text{sr}^{-1}$. We have then extrapolated the differential source counts using a power law fitting the fainter flux bins (slope = -0.58) to obtain an estimate of the expected value of the total background at 24 μm : $2.016 \text{ nWm}^{-2}\text{sr}^{-1}$. The fraction of the background that we resolve down to $38 \mu\text{Jy}$ is about 62%.

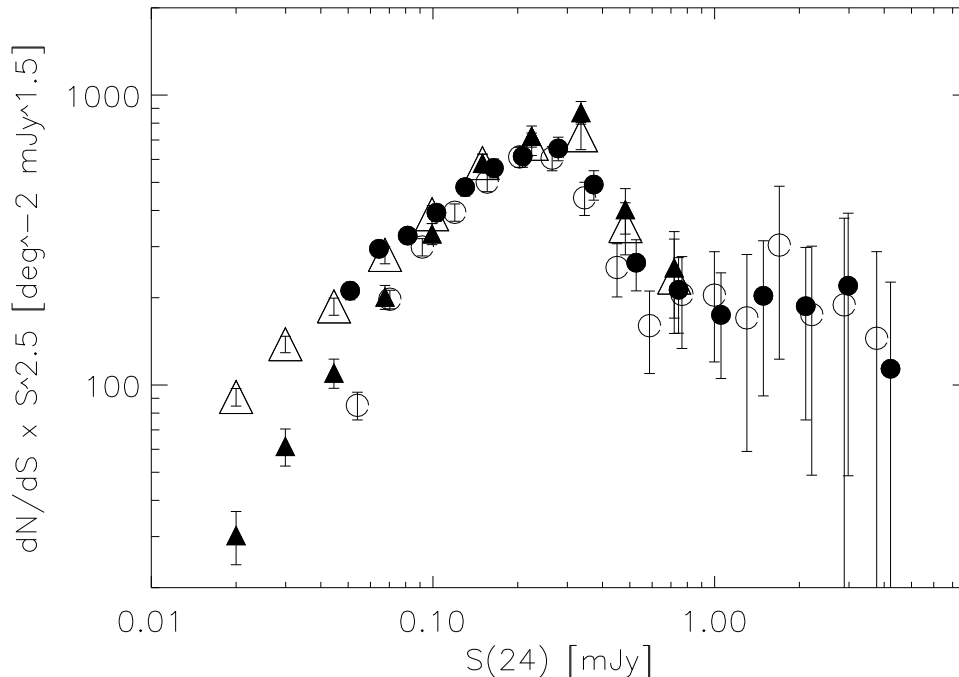


Figure 7. Differential 24 μm counts normalized to the Euclidean law ($N \propto S^{-2.5}$). We compare the distribution obtained by using our final deblended catalogue (filled circles, 983 sources) and the preliminary 5- σ catalogue prior to deblending (open circles, 953 sources). We compare our results with the source counts by Chary et al. (2004). The filled triangles refer to their uncorrected counts, the open triangles correspond to their final completeness corrected data.

Papovich et al. (2004) report a value for the total background intensity at 24 μm of $2.7 \text{ nW m}^{-2} \text{ sr}^{-1}$, a factor of $\sim 30\%$ higher than our estimate.

6 SUMMARY

We have analysed a deep MIPS 24 μm survey in the EN1 region, conceived as a validation observation for the official GOODS strategy (Dickinson et al. 2004). The archival Spitzer data of the GOODS EN1 test field allowed us to check the effects of source confusion on the mid-IR statistics. We have processed the data to obtain a final mosaic that is basically confusion limited. To deal with confusion, we have applied the CLEAN algorithm to the 24 μm map, removing the diffraction rings around bright sources. Few blend sources are then partially recovered and appear as resolved objects in the CLEANed map. A different approach is needed for confused sources with closer counterparts. We used the information from higher frequency observations in the same regions in order to detect the counterparts of the apparently extended 24 μm blend sources. An optimal solution is provided by the near-IR camera on board Spitzer, IRAC. In particular, we have referred to the 3.6 μm and 4.5 μm maps to associate the single counterparts to the sub-components of the 24 μm unresolved emission. An optical R-band image (Fadda et al. 2004) has also been considered for disentangling a few dubious cases. We have then obtained a reliable 24 μm catalogue including 983 sources at the 5- σ level, the fainter source reaching a flux of 23 μJy . We have

shown that our sample is almost unbiased down to $\sim 40 \mu\text{Jy}$, and that by applying a deblending procedure we do not need to apply any statistical completeness correction (at least to the flux level considered). This is probed by direct comparison of our results with those of Chary et al. (2004), who analysed the same data-set through extensive Monte Carlo simulations.

We have estimated the confusion limit of the MIPS 24 μm survey using the classical level definition of 30 independent beams per source, obtaining a value of 77 μJy . We also found that the deblending procedure has reduced of about 30% the confusion noise.

We have compared the 24 μm extragalactic source counts derived from our sample with those published by Chary et al. (2004) and Papovich et al. (2004). We found a good agreement between the different data-sets, when reporting the counts of the other authors to the same flux scale. At the bright end, the GOODS EN1 test field is biased by low statistics and probably cosmic variance, resulting in an underdensity of bright sources at $> 0.3 \text{ mJy}$ with respect to larger area surveys (Papovich et al. 2004).

By extrapolating the source counts to fainter fluxes, we have estimated the fraction of the cosmic background already resolved by our sample down to a flux level of 38 μJy : $\sim 62\%$.

The main goal of this work was to provide a reliable catalogue of mid-IR sources. This is essential in order to study the physical nature of the fainter population responsible for most of the cosmic IR background.

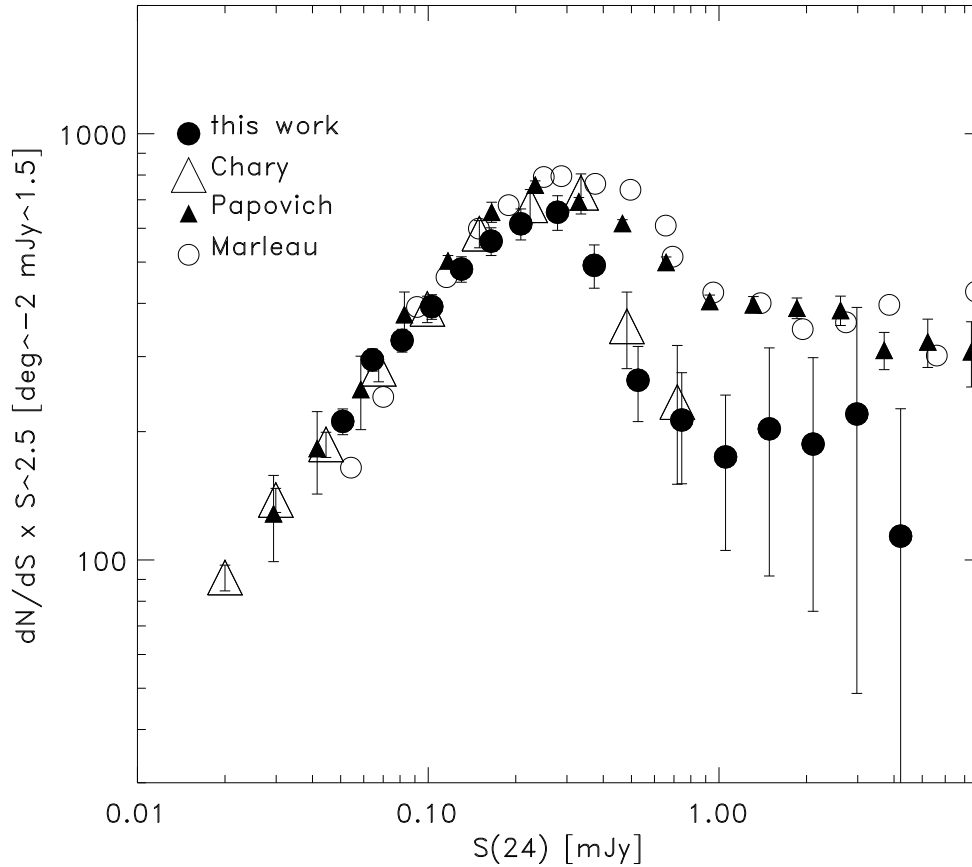


Figure 8. Differential 24 μm counts normalized to the Euclidean law. We compare our source counts (filled circles) with those of Chary et al. (2004, open triangles), Papovich et al. (2004, filled triangles) and Marleau et al. (2004, open circles).

REFERENCES

- Bertin, E., Arnouts, S., 1996, *A&AS*, 117, 393
Chary, R., Casertano, S., Dickinson, M. E., Ferguson, H. C., Eisenhardt, P. R. M., Elbaz, D., Grogin, N. A., Moustakas, L. A., Reach, W. T., Yan, H. 2004, *ApJS*, 154, 80
Dole, H., Lagache, L., Puget, J.L. 2005, to appear in "The Spitzer Space Telescope: New Views of the Cosmos", conference proceedings held November 2004 in Pasadena, Eds L. Armus, astro-ph/0503017
Dickinson, M. 2004, *AAS*, 205
Dole, H., Rieke, G. H., Lagache, G. et al. 2004, *ApJS*, 154, 93
Dole, H., Lagache, G., Puget, J.-L. 2003, *ApJ*, 585, 617
Elbaz, D., Cesarsky, C. J., Fadda, D. et al., 1999, *A&A* 351, L37
Fadda, D., Jannuzi, B.T., Ford, A., Storrie-Lombardi, L. J. 2004, *AJ*, 128, 1
Fazio, G. G., Hora, J. L., Allen, L. E. et al. 2004, *ApJS*, 154, 10
Franceschini, A., Berta, S., Rigopoulou, D. et al., 2003, *A&A*, 403, 501
Hauser M. G. & Dwek E., 2001, *ARA&A*, 39, 249
Lonsdale, C.J., Polletta, M., Surace, J. et al. 2004, *ApJS*, 154, 54
Lonsdale, C.J., Smith, H.E., Rowan-Robinson, M. et al. 2003, *PASP*, 115, 897
Marleau, F. R.; Fadda, D.; Storrie-Lombardi, L. J.; Helou, G.; Makovoz, D.; Frayer, D. T.; Yan, L.; Appleton, P. N.; Armus, L.; Chapman, S.; Choi, P. I.; Fang, F.; Heinrichsen, I.; Im, M.; Lacy, M.; Shupe, D.; Soifer, B. T.; Squires, G.; Surace, J.; Teplitz, H. I.; Wilson, G. 2004, *ApJS*, 154, 66
Papovich, C., Dole, H., Egami, E. 2004, *ApJS*, 154, 70
Rieke, G. H., Young, E. T., Engelbracht, C. W. et al. 2004, *ApJS*, 154, 25
Rodighiero, G., Lari, C., Fadda, D., Franceschini, A., Elbaz, D., Cesarsky, C. 2004, *A&A*, 427, 773

Table 1. First 10 entries of the 24 μm source catalogue in the EN1 test field

ID	RA	DEC	S/N	S(24 μm) [μJy]
EN1-160855+550112	16:08:55.87	55:01:12.05	194	2990
EN1-160942+550009	16:09:42.66	55:00:09.48	191	1597
EN1-160906+545557	16:09:06.53	54:55:57.38	94	747
EN1-160904+545821	16:09:04.47	54:58:21.75	94	1067
EN1-160848+545150	16:08:48.87	54:51:50.46	92	1194
EN1-160936+550242	16:09:36.91	55:02:42.39	69	557
EN1-160921+545109	16:09:21.50	54:51:09.93	62	700
EN1-160839+545523	16:08:39.85	54:55:23.39	62	553
EN1-161003+545344	16:10:03.27	54:53:44.77	57	803
EN1-160839+545523	16:08:39.85	54:55:23.39	54	553